doi:10.1038/nature13230

Sea-level and deep-sea-temperature variability over the past 5.3 million years

E. J. Rohling[1,2], G. L. Foster[2], K. M. Grant[1], G. Marino[1], A. P. Roberts[1], M. E. Tamisiea[3] & F. Williams[2]

Ice volume (and hence sea level) and deep-sea temperature are key measures of global climate change. Sea level has been documented using several independent methods over the past 0.5 million years (Myr). Older periods, however, lack such independent validation; all existing records are related to deep-sea oxygen isotope ($\delta^{18}O$) data that are influenced by processes unrelated to sea level. For deep-sea temperature, only one continuous high-resolution (Mg/Ca-based) record exists, with related sea-level estimates, spanning the past 1.5 Myr. Here we present a novel sea-level reconstruction, with associated estimates of deep-sea temperature, which independently validates the previous 0–1.5 Myr reconstruction and extends it back to 5.3 Myr ago. We find that deep-sea temperature and sea level generally decreased through time, but distinctly out of synchrony, which is remarkable given the importance of ice-albedo feedbacks on the radiative forcing of climate. In particular, we observe a large temporal offset during the onset of Plio-Pleistocene ice ages, between a marked cooling step at 2.73 Myr ago and the first major glaciation at 2.15 Myr ago. Last, we tentatively infer that ice sheets may have grown largest during glacials with more modest reductions in deep-sea temperature.

To understand better the potential response of ice volume (sea level) to global warming, there is a need for continuous, highly resolved and well-quantified records of sea-level variations associated with past climate fluctuations[1–4]. In addition, such records are critical for understanding the development of major ice-age cycles over the past ~3 Myr and of the attendant reorganizations in the coupled climate–ocean system, including extensive biological and biogeochemical perturbations[5–8].

Continuous sea-level records with centennial resolution, suitable for investigating magnitudes and rates of sea-level change, exist for the past 0.5 Myr (refs 1, 9–11). For older periods, existing millennially resolved sea-level reconstructions include (1) a continuous, model-based deconvolution of global deep-sea benthic foraminiferal $\delta^{18}O$ data ($\delta^{18}O_b$) into temperature and ice-volume changes back to 35 Myr ago[12]; (2) a scaling of global deep-sea $\delta^{18}O_b$ using New Zealand sequence stratigraphic data for 3.4–2.3 Myr ago[2,3]; (3) a direct scaling of another deep-sea $\delta^{18}O_b$ compilation for the past 7 Myr (ref. 13); and (4) a deep-sea $\delta^{18}O_b$ record (corrected for deep-sea temperature, T_{ds}) over the past 1.5 Myr from Chatham rise, in the southwest Pacific Ocean, which is argued to be representative of global deep water[14]. A further, lower-resolution, T_{ds}-corrected deep-sea $\delta^{18}O_b$ record exists for the North Atlantic[15], although questions exist concerning carbonate chemistry influences on the epibenthic species analysed in that record[16], and about site-specific issues regarding North Atlantic Deep Water property variations versus potential water-mass changes due to Antarctic Bottom Water penetration.

All existing methods rely on deep-sea $\delta^{18}O_b$ and are, therefore, not independent of each other. In addition, there is limited temporal overlap between these reconstructions and, importantly, methodological uncertainties are typically much larger in sea-level reconstructions for periods before 0.5 Myr ago. Hence, it is necessary to develop independent sea-level reconstructions to identify mutually consistent patterns. This in turn will enable fundamental questions to be addressed concerning the timing and development of Northern Hemisphere glaciation, sea-level variability during past warm periods with greenhouse gas concentrations similar to those of today, and the long-term relationship between ice volume, temperatures and greenhouse gas concentrations. To advance the debate, we here present a new and independent sea-level reconstruction that spans the past 5.3 Myr.

Location for new sea-level reconstruction

The Red Sea would be a promising location for developing an extended sea-level reconstruction beyond 0.5 Myr ago[1,10,11,17]. Red Sea sea-level reconstructions for the past 0.5 Myr rely on hydraulic control of water exchange through a shallow and narrow connection with the open ocean (the Bab-el-Mandab Strait)[10,17]. The method is independent of deep-sea $\delta^{18}O_b$, and yields 'Relative sea level at Bab-el-Mandab' (RSL_{BeM}) reconstructions with a 1σ uncertainty of ~6 m (refs 10, 17). Unfortunately, no high-quality Red Sea sediment cores exist that allow extension of RSL_{BeM} beyond 0.55 Myr ago. We therefore shift focus to the Mediterranean Sea, which is another evaporative marginal sea with limited connection to the open ocean.

Discerning a sea-level signal in Mediterranean records of carbonate microfossil $\delta^{18}O$ is more complex than in the Red Sea because (1) the larger strait profile at Gibraltar, relative to Bab-el-Mandab, causes a lower signal-to-noise ratio, with Mediterranean glacial–interglacial $\delta^{18}O$ amplitudes of 2.5–3‰ compared to Red Sea amplitudes of 5.5–6‰; and (2) the Mediterranean hydrological cycle is more complicated than in the Red Sea, with major rivers that integrate information from a large catchment area with influences from both temperate climate conditions and the African monsoon[10,11,17–19]. However, the Mediterranean provides uninterrupted sediment records dating back to the end of the Messinian salinity crisis at 5.33 Myr ago, from tectonically uplifted marine sediments and long deep-sea sediment cores[20,21]. Eastern Mediterranean planktonic foraminiferal $\delta^{18}O$ records ($\delta^{18}O_p$) have recently been synthesized into a 5.3-Myr 'Mediterranean stack' with a millennially resolved, orbitally tuned chronology[22]. It is particularly beneficial for sea-level reconstruction that orbital tuning of the Mediterranean record (in contrast to deep-sea $\delta^{18}O_b$ records) makes no assumptions about the relationship between insolation and ice volume; instead, it employs a timing relationship between insolation and African monsoon intensity (using sedimentary cycles)[20]. The Mediterranean chronology is so

[1]Research School of Earth Sciences, The Australian National University, Canberra 0200, Australia. [2]Ocean and Earth Science, University of Southampton, National Oceanography Centre, Southampton SO14 3ZH, UK. [3]National Oceanography Centre, Joseph Proudman Building, Liverpool L3 5DA, UK.

well established that it underpins global geochronology throughout the time interval considered here[20,23]. Therefore, the eastern Mediterranean $\delta^{18}O_p$ stack[22] is an excellent resource for developing a long sea-level record using a Mediterranean version of the method that was developed for the Red Sea (see Methods). This has only recently become possible owing to increased quantitative understanding of the relationship between hydrological processes and $\delta^{18}O$ changes in and around the Mediterranean[11,18,19,24].

Converting Mediterranean $\delta^{18}O$ to sea level

We quantify relative sea-level changes at Gibraltar (RSL_{Gib}) using values of eastern Mediterranean $\delta^{18}O_p$ after removal of 'sapropel' intervals of major surface freshwater dilution. These intervals are associated with periods of sea-floor anoxia and are typically marked by dark olive to black organic-rich sediments (bounded by pale organic-poor deposits), with light surface-water $\delta^{18}O$ anomalies, elevated sedimentary Ba/Al ratios and an absence of benthic microfossils[19,21,25–29]. We exclude sapropel intervals from RSL_{Gib} on the basis of a combination of $\delta^{18}O_p$ anomaly detection and visual evidence (Extended Data Fig. 1).

Our RSL_{Gib} reconstruction method is explained in detail in Methods (with code in Supplementary Information). The method exploits the influences of sea-level and buoyancy-loss changes on a hydraulic control model[30] for the Strait of Gibraltar[18,25,31], which has been independently validated (within uncertainties) by other analytical and numerical solutions[32–35]. The strait model is connected to a basin-representation box model, which includes summer and winter mixed-layer separation, and oxygen isotope fractionation calculations[18,19]. The basin model is identical to that detailed in ref. 19, except that we here omit the so-called 'monsoon box', which is relevant only to sapropels (which are excluded here). Following previous Mediterranean habitat identifications[19], two $\delta^{18}O_p$-to-RSL 'converters' are presented: one for (upper) Mediterranean Intermediate Water dweller *Neogloboquadrina pachyderma* (dextral); and one for summer mixed-layer dweller *Globigerinoides ruber* (white). These 'converters' (notably that for *G. ruber*) are here used to determine changes in RSL_{Gib} from non-sapropelic eastern Mediterranean $\delta^{18}O_p$ data (Extended data Fig. 2). Propagated uncertainties in individual RSL_{Gib} estimates are up to ~20 m (1σ; see Fig. 1 and Methods), but uncertainty in the mean signal is smaller owing to autocorrelation in the record. A probabilistic assessment that combines RSL_{Gib} uncertainties with chronological uncertainties yields a 'probability maximum' record with a 95% probability interval of ±6.3 m (see Fig. 2 and Methods).

The RSL_{Gib} method relies on two underlying assumptions. The first is that the Strait of Gibraltar in the past has exerted hydraulic control on water exchange in a similar manner to today[30]. Large-scale tectonic movement would be detected as a breakdown, or major drift, in the sea-level solutions. Given that the Strait of Gibraltar probably formed during a terminal Miocene event that may have been followed by intense crustal adjustments and erosion[36,37], it is best to consider the earliest portion of RSL_{Gib} with caution. In the interval younger than 3.3 Myr, confidence increases owing to comparison with other sea-level reconstructions (see below), and because of indications that exchange flow through the Strait of Gibraltar adopted a modern-type configuration from about 3.8 Myr ago[38] (Methods). The second assumption concerns our $\delta^{18}O$-to-RSL 'converter'. It relies on Late Pleistocene parameter relationships with generous uncertainty ranges (Methods), and assumes that past relationships remained within these uncertainty ranges. Again, we expect deviations from this assumption to cause a breakdown, or major drift, in the solutions. Validation between RSL_{Gib} and independent methods suggests that this assumption is valid, especially in the past 1.5 Myr and probably throughout (at least) the past 3.3 Myr (Figs 1, 2). Nonetheless,

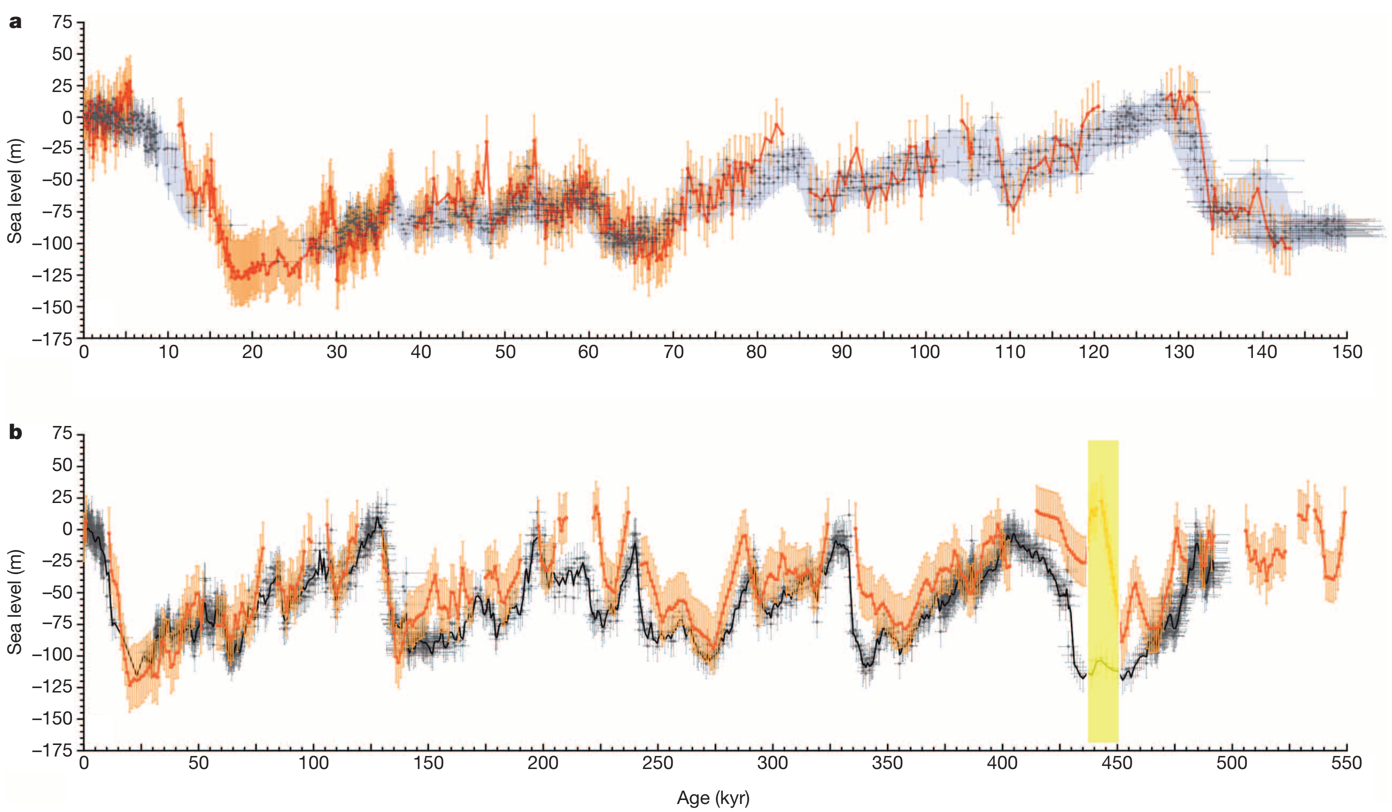

Figure 1 | RSL_{Gib} compared with RSL_{BeM}. RSL_{BeM} has been previously validated against a wide range of independent sea-level benchmarks[1,10,11]. **a**, RSL_{Gib} for eastern Mediterranean sediment core LC21 (red) with 1σ error bars (orange), and RSL_{BeM} (black) with 2σ error bars[1,11,40] as well as the probabilistically assessed 95% probability envelope (shading)[11]. Individual Mediterranean data comply with the 2σ envelope for the Red Sea data. **b**, RSL_{Gib} for an eastern Mediterranean stack[22] (red) with 1σ error bars (orange), and RSL_{BeM} (black) with 2σ error bars[1,11,40]. Gaps in the RSL_{Gib} records result from removal of sapropel(-like) events, but some residual influences of freshwater influxes on Mediterranean $\delta^{18}O$ (ref. 19) may remain immediately adjacent to these intervals. An apparent 'undetected' sapropel-like event (yellow bar) is also indicated (Methods). Note that **a** and **b** cover different age ranges.

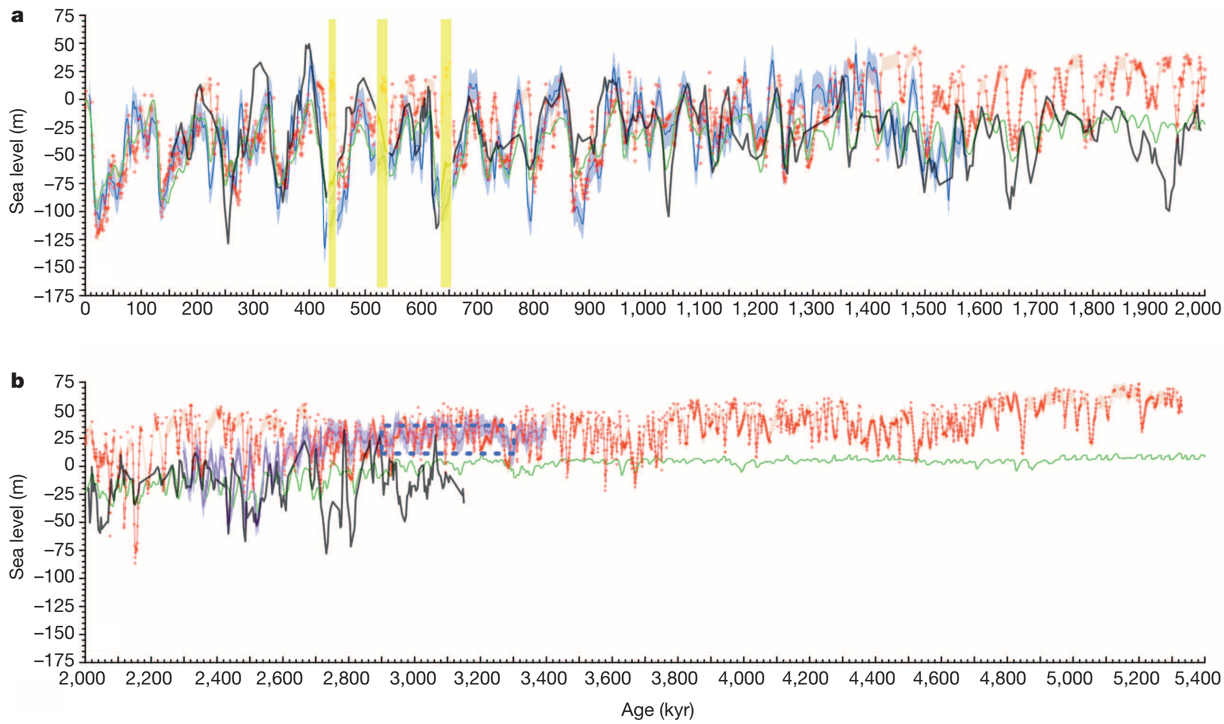

Figure 2 | RSL_{Gib} for an eastern Mediterranean $\delta^{18}O_p$ stack, compared with other sea-level estimates. **a**, Interval from 0 to 2 Myr ago. **b**, Interval from 2 to 5.4 Myr ago. RSL_{Gib} (based on the record of ref. 22) is presented using all non-sapropelic data points (red dots), along with the median (red line) from probabilistic analysis with its 95% probability interval (light orange shading). In sapropel intervals, marked by absence of (red) data points, linear interpolation of the 95% probability interval is shown for aesthetic reasons only (Methods). Other sea-level estimates are from Mg/Ca-based T_{ds}-corrected deep-sea $\delta^{18}O_b$ for the southwest Pacific[14] (blue; see Methods for its probabilistic presentation here) and for the North Atlantic[15] (black; 3-point moving average); a model-based deconvolution of deep-sea $\delta^{18}O_b$ (ref. 12) (green); and conversion of deep-sea $\delta^{18}O_b$ with support from New Zealand sequence stratigraphic data[2,3] (purple). The last was vertically positioned to agree with the 12–32 m ESL estimate for the period 2.9–3.3 Myr ago (ref. 3; dark blue dashed box). Three apparent 'undetected' sapropel-like intervals in RSL_{Gib} are indicated (yellow bars; Methods).

given the potential caveats to our method with respect to long-term tectonic and climate-regime changes, we emphasize the need for new continuous and highly resolved records from independent methods to strengthen mutual validations before 1.5 Myr ago, and especially before 3.3 Myr ago (Methods).

We also make an initial assessment of land movement due to glacio-hydro-isostatic adjustment at the Camarinal sill, which is the shallowest and hydraulically limiting passage on the Atlantic side of the Gibraltar narrows[30] (Methods). We find that the glacial–interglacial amplitude of RSL_{Gib} underestimates global mean (eustatic) sea level (hereafter ESL), and that the offset scales proportionally with the variation in land ice (where ESL = 1.23 RSL_{Gib}; see Methods), so that ESL amplitude variations will be larger than those of RSL_{Gib}. This scaling suggests Pliocene isostatic adjustments in the region that are compatible with previous estimates[39]. Regardless, in our comparisons with estimates from other methods (Figs 1 and 2), we plot RSL_{Gib} instead of ESL, because issues about extension of our isostatic assessment back in time, and to periods with sea level considerably above the present level, remain to be constrained. We note that the current best estimate for ESL in the period 3.3–2.9 Myr ago is in the range 12–32 m (ref. 3), similar to the Pliocene range of 9–31 m used in ref. 4. These values agree well with RSL_{Gib} fluctuations during that period (Fig. 2). The previous estimates do not specify the nature and magnitude of temporal variability, so our RSL_{Gib} record provides the first quantitative view of the secular evolution of sea level during the Pliocene that is independent of deep-sea $\delta^{18}O_b$.

RSL_{Gib} validation

Where overlap exists, comparison of RSL_{Gib} with independent sea-level reconstructions reveals good agreement (Figs 1 and 2). For younger intervals (<0.5 Myr ago), we now assess RSL_{Gib} values derived from different $\delta^{18}O_p$ data sets on their respective timescales. RSL_{Gib} from $\delta^{18}O_p$ in eastern Mediterranean sediment core LC21—which has a closely related chronology to RSL_{BeM}[11]—agrees well with RSL_{BeM} over the last glacial cycle through intervals of both deglaciation (145–125 kyr ago) and glacial inception (120–65 kyr ago), and has the additional benefit of resolving changes between 26 and 14 kyr ago, where RSL_{BeM} is poorly resolved due to aplanktonic conditions in the Red Sea (Fig. 1a). Using an eastern Mediterranean $\delta^{18}O_p$ stack[22], and allowing for different age models, RSL_{Gib} also compares well with RSL_{BeM} over the past 0.5 Myr (refs 1, 40; Fig. 1b). Agreement between the two RSL records from different ocean margins reflects the fact that both areas have generally comparable glacio-hydro-isostatic responses (Methods). The principal disagreements lie close to sapropel(-like) intervals of freshwater dilution in the Mediterranean, which tend to bias RSL_{Gib} towards higher values. This suggests that residual effects of these events may occasionally remain, owing to imperfect detection/removal of sapropel(-like) intervals (Methods). Future work can use same-sample multi-proxy approaches to improve this situation, and reinstate the 'monsoon box' in the model[19] to try and resolve RSL_{Gib} through sapropel intervals, but these are multi-year efforts beyond the scope of the present study (Methods).

Next we compare the full RSL_{Gib} record with available sea-level reconstructions for older (>0.5 Myr ago) intervals (Fig. 2). We observe strong agreement between RSL_{Gib} and sea-level estimates from Mg/Ca T_{ds}-corrected deep-sea $\delta^{18}O_b$ over the past 1.5 Myr (ref. 14; Fig. 2a), which independently supports the intensification of glacials across the Mid-Pleistocene transition that was first inferred from the southwest Pacific T_{ds}-corrected deep-sea $\delta^{18}O_b$ record[14]. However, before ~1.5 Myr ago, highstand values of RSL_{Gib} seem higher than those in other studies[14,15]. Apart from RSL_{Gib}, the only records with continuity across the past 3 Myr are an Atlantic T_{ds}-corrected deep-sea $\delta^{18}O_b$ record[15], and the model-based estimates of ref. 12. Relative to RSL_{Gib}, both suggest a lower mean sea level between ~1.5 and 3.2 Myr ago (Fig. 2). If we assume that this difference arises from bias in RSL_{Gib}, then it might reflect a more open strait before ~1.5 Myr ago, possibly due to an uplift event in the Strait of Gibraltar at ~1.5 Myr ago. However, such an event would also affect the sea-level sensitivity (amplitude response) of Mediterranean $\delta^{18}O$. This is difficult to reconcile with the observation that RSL_{Gib} amplitude variations agree well with those in a record based on scaling of a New Zealand sequence stratigraphic record between 3.4 and 2.3 Myr ago[2,3], and also with those in the Atlantic record (allowing for resolution and chronological differences)[15] (Fig. 2b). Hence, we suggest that any change in RSL_{Gib} at ~1.5 Myr ago is more likely to reflect a 'baseline shift' in Mediterranean climate conditions from a warm/moist state to a warm/arid state, rather than a tectonic step at the Strait of Gibraltar. Alternatively, we might assume that the bias is not due to RSL_{Gib}, given that there is good agreement between RSL_{Gib} and previous sea-level range estimates for the 2.9–3.3 Myr interval (Fig. 2b). That would suggest that problems may instead lie within the Atlantic T_{ds}-corrected deep-sea $\delta^{18}O_b$ record[15] (as also suggested before; see, for example, ref. 16), and within the model-based estimates of ref. 12. Further independent validation is needed before this can be settled, but—regardless—major signal-amplitude similarity in all independent observational methods over the past 3.3 Myr challenges the substantially different sea-level inferences from model-based deconvolution of deep-sea $\delta^{18}O_b$ (ref. 12; Fig. 2a, b).

Deep-water temperature variability

Next, we use RSL_{Gib} to derive information about global T_{ds} changes. Owing to uncertainty in the long-term RSL_{Gib}:ESL scaling, we consider two scenarios, one of which relies on direct use of RSL_{Gib} and the other on an ESL estimate of 1.23 × RSL_{Gib} (Figs 3, 4). We translate these into estimates of seawater $\delta^{18}O$ ($\delta^{18}O_w$) changes using a ratio of (0.009 ± 0.001)‰ m^{-1} (refs 14, 41, 42; Figs 3b and 4b). Subtraction of $\delta^{18}O_w$ from a global deep-sea $\delta^{18}O_b$ stack[43] (Figs 3a and 4a), following slight adjustment of the chronology of this stack to that of the RSL_{Gib} record (Methods; Extended Data Table 1), yields residuals that approximate global T_{ds} changes in a 0.25‰ °C^{-1} ratio[14]. Thus, we estimate global T_{ds} changes over the past 5.3 Myr, with propagated (2σ) uncertainties of about ±0.6 °C (Figs 3c and 4c). Our estimates agree well with independent Mg/Ca-based T_{ds} estimates for a site that is thought to approximate global mean deep-water conditions[14] (Figs 3c and 4c). The observed mutual consistency over glacial–interglacial cycles and longer timescales between this Mg/Ca-based T_{ds} record and associated sea-level reconstruction[14], and our RSL_{Gib} and associated T_{ds} reconstruction, suggests that over the past 1.6 Myr (1) seawater Mg/Ca ratios did not change significantly and (2) Strait of Gibraltar morphology and the Mediterranean 'baseline climate state' experienced no major changes. In addition, the lower-resolution Atlantic T_{ds} record[15] also validates a major T_{ds} drop in our reconstruction at ~2.73 Myr ago (see below; Fig. 3c).

Timing and magnitude of glaciations

Several key observations can be drawn from our analysis. First, we extend to 5.3 Myr ago the conclusion, previously drawn for the past 1.5 Myr (ref. 14), that global deep-sea $\delta^{18}O$ (see, for example, refs 13, 43) does not adequately capture ice-volume history because its two main components (T_{ds} and ice-volume effects) underwent distinctly different temporal developments (Fig. 3). Second, regarding the onset of Quaternary glacial cycles, we find that a distinct deep-sea cooling step at 2.73 Myr

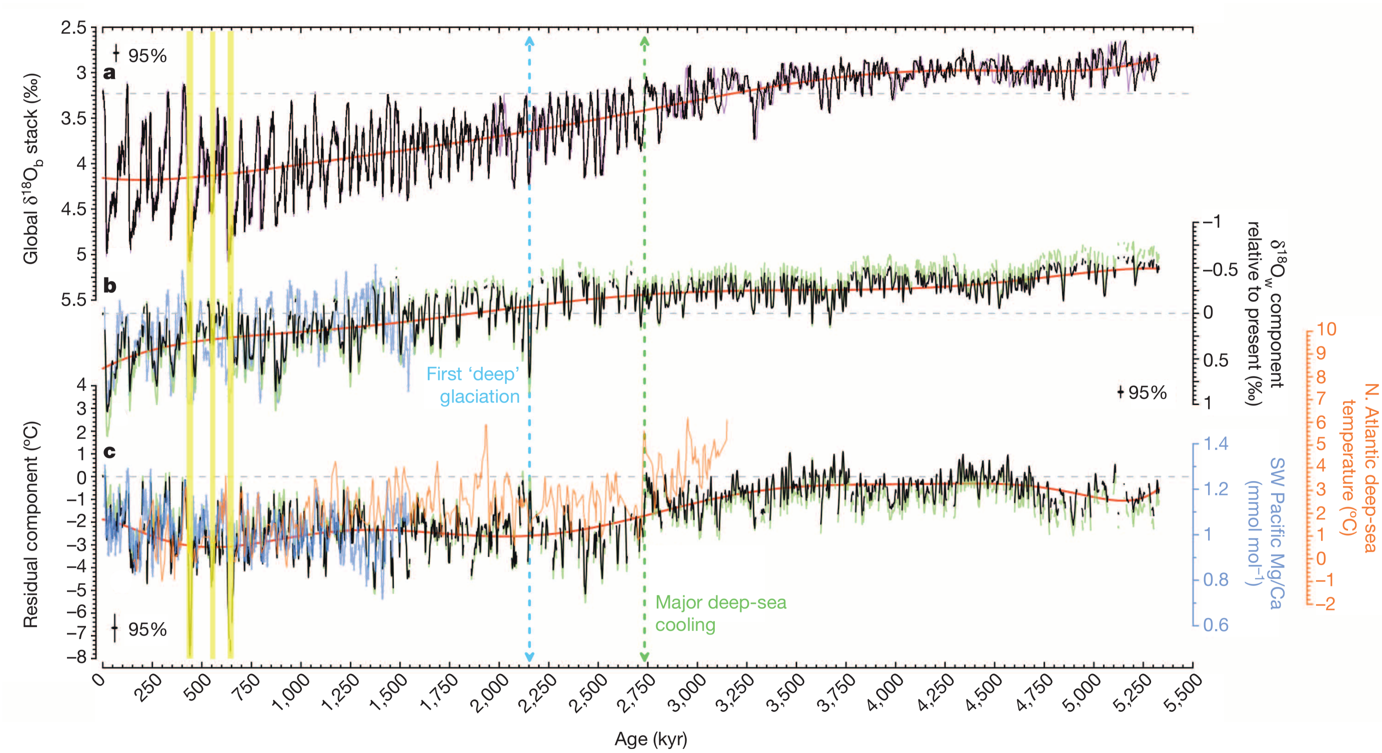

Figure 3 | Deep-sea temperature and $\delta^{18}O_w$ components of deep-sea $\delta^{18}O_b$. **a**, Deep-sea $\delta^{18}O_b$ (ref. 43) on original chronology (magenta) and chronology tuned to that of ref. 22 (black). **b**, Component of sea-level-based ocean $\delta^{18}O_w$ variations (in black based on RSL_{Gib} and in green for our ESL approximation, both using 0.009‰ m^{-1}), compared with $\delta^{18}O_w$ for the southwest Pacific[14] (blue; 3-point moving average). All variations are assessed relative to present. **c**, Residual $\delta^{18}O$ component that is ascribed to T_{ds} changes using 0.25‰ °C^{-1}. Gaps in **b** and **c** relate to sapropel(-like) intervals. For details see Methods. Also shown in **c** are 3-point moving averages of Mg/Ca-based T_{ds} records for the North Atlantic[15] (orange) and the southwest Pacific (blue)[14]. The southwest Pacific record is shown in original Mg/Ca units (as made available), but is exactly scaled to T_{ds} variations on the other axes as described in ref. 14. Error bars: **a**, mean uncertainties reported for deep-sea $\delta^{18}O_b$ in the global stack[43]; **b**, propagated uncertainty in the sea-level (RSL_{Gib})-based $\delta^{18}O_w$ change component, based on the 95% probability envelope to the median (Methods, and Fig. 2) and a ±0.001‰ m^{-1} uncertainty in the conversion to $\delta^{18}O_w$; and **c**, propagated uncertainties from **a** and **b**. Yellow bars as in Fig. 2. A major deep-sea cooling (green dashed line), and the first 'deep' glaciation (sea-level lowering below −70 m; blue dashed line) are indicated. Red lines are straightforward polynomial fits shown only to highlight general long-term trends (all based directly on RSL_{Gib}). Age on *x* axis is based on the chronology of ref. 22. A magnification of the past 1.5 Myr is shown in Fig. 4.

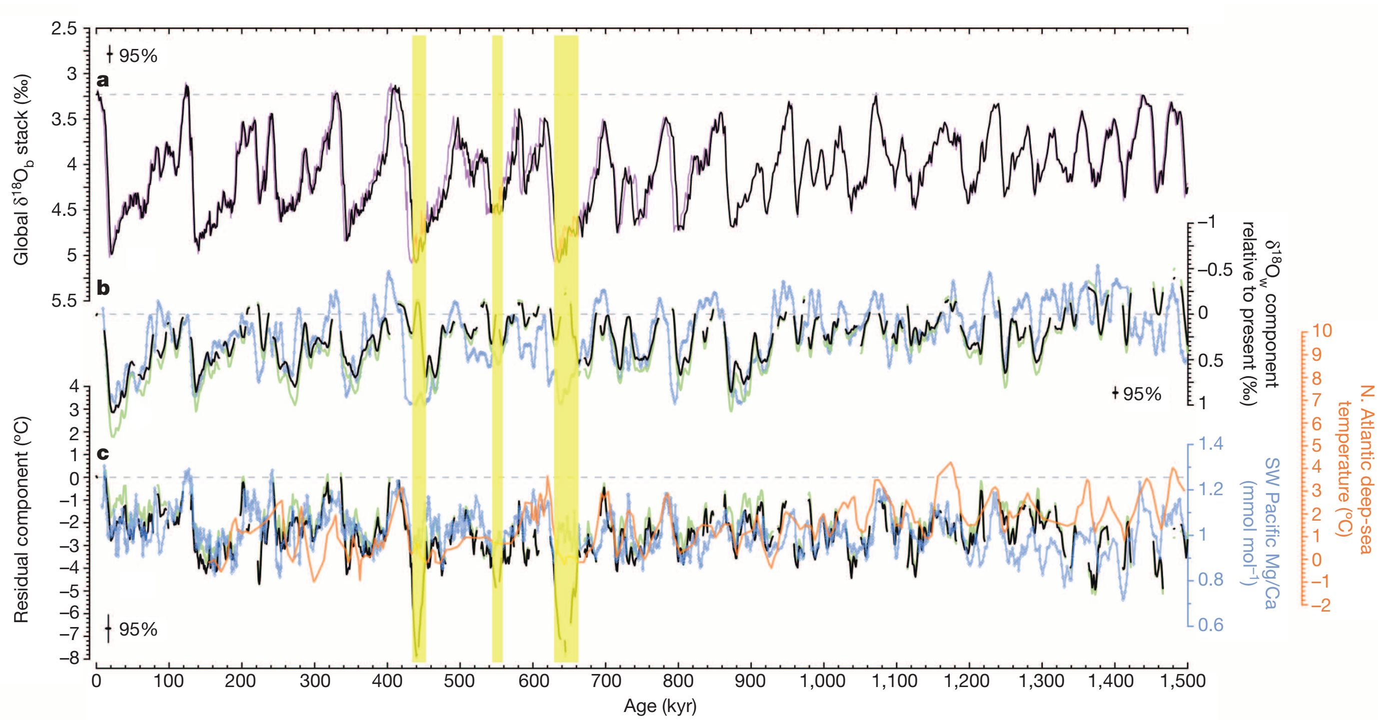

Figure 4 | Expanded version of Fig. 3 for the past 1.5 Myr only. a–c, As in Fig. 3. Error bars: **a**, mean uncertainties reported for deep-sea $\delta^{18}O_b$ in the global stack[43]; **b**, propagated uncertainty in the sea-level (RSL_{Gib})-based $\delta^{18}O_w$ change component, based on the 95% probability envelope to the median (Methods, and Fig. 2) and a $\pm 0.001‰ \, m^{-1}$ uncertainty in the conversion to $\delta^{18}O_w$; and **c**, propagated uncertainties from **a** and **b**.

ago substantially pre-dated the first major glaciation in our record, by 0.58 Myr (Fig. 3). Note that bias due to sapropel intervals is towards high RSL_{Gib} values, and that comparisons between well-defined RSL_{Gib} lowstand values are robust relative to this bias. This strengthens confidence in our identification of the first major lowstand, especially because data for the event at 2.15 Myr ago appear to be ~60 m (3σ) lower than for any preceding lowstand (Fig. 2).

Current concepts for the onset of Northern Hemisphere glaciation rely strongly on deep-sea $\delta^{18}O_b$ data, and suggest a shift to stronger glacials at ~2.7–2.5 Myr ago (refs 43, 44; Fig. 3a). Our new data challenge this perspective, because the change at 2.73 Myr ago appears to relate to cooling, whereas the first 'deep' (sea level below −70 m) glacial occurred considerably later, at 2.15 Myr ago. Pronounced cooling at ~2.73 Myr ago is supported not only by the independent Atlantic deep-sea Mg/Ca record[15] (Fig. 3c), but also by an alkenone-based North Atlantic surface temperature record[6], and the culmination of a long-term equatorial Pacific cooling trend[45]. It is consistent with ample evidence for widespread ocean and climate change at ~2.7 Myr ago (Extended Data Table 2), including glaciation on Greenland and Scandinavia (see synthesis in ref. 8). Apparent temporal association of this cooling with a decline in atmospheric CO_2 levels (see, for example, ref. 46) suggests a causal link. For instance, stratification in both the North Pacific and the Southern Ocean intensified at ~2.7 Myr ago in association with deep-sea cooling, leading to increased ocean carbon storage[5]. These are key regions of deep and intermediate water formation (particularly the Southern Ocean), and changes in their overturning circulation may, therefore, strongly influence widespread oceanic carbon storage and, hence, atmospheric CO_2 levels (see, for example, ref. 47). Our inferred first 'deep' glacial at 2.15 Myr ago also falls within a window of major climatic and oceanic changes (Extended Data Table 2), including a major cooling in tropical sea surface temperatures[48], but its nature requires further validation (for example, through extension of the record of ref. 14).

Terrestrial indications that a major North American ice sheet developed to low latitudes (39° N) date to ~2.4 Myr ago, while the earliest record of significant North American-sourced ice-rafted debris suggests that ice sheets extended to marine margins at 2.64 Myr ago (refs 7, 8). RSL_{Gib} has amplitudes of 50–70 m at that time (Fig. 2b), which imply that early ice sheets had relatively low profiles relative to their large inferred areas. Such 'low-slung' ice sheets may have existed because basal friction was lower during early glacial cycles than during more recent ones[49,50].

Finally, we infer that similar amplitudes among three of the last four glacial maxima in the global deep-sea $\delta^{18}O_b$ stack[43] (Figs 3a and 4a) may obscure increasing ice-volume contributions (Figs 3b and 4b) that are compensated by decreasing deep-sea temperature contributions (Figs 3c and 4c). Two independent methods (this Article and ref. 14) suggest that the Last Glacial Maximum was one of the most intense glaciations in terms of ice volume, but that its deep-sea temperatures may have been relatively 'mild' by glacial standards (Figs 3 and 4). This apparent difference in T_{ds} between glacials is smaller in the southwest Pacific record[14] than in our reconstruction (Fig. 4); possibly, it was most notable in the Atlantic Ocean, which dominates the $\delta^{18}O_b$ stack[43] that we used to estimate T_{ds}. The pattern also is less evident in RSL_{BeM}, but RSL_{BeM} is known to be deficient through the LGM[10,17] (Fig. 1). At this stage, therefore, the inferred pattern is suggestive only; it requires validation from both improved RSL_{Gib} reconstructions based on continuous multi-proxy core records, and additional deep-sea benthic Mg/Ca records. If validated, then it may reflect the importance of atmospheric moisture supply (and reduced atmospheric moisture capacity with decreasing temperature) in determining total ice accumulation.

METHODS SUMMARY

In Methods, we explain (1) our Mediterranean relative sea level at Gibraltar (RSL_{Gib}) calculations, including elimination of so-called sapropelic intervals with freshwater dilution, a discussion of long-term tectonic effects, an assessment of glacio-hydro-isostatic influences and an outline of scope for future refinements; (2) our probabilistic assessment of the sea-level record of ref. 14; and (3) our use of RSL_{Gib} with the deep-sea $\delta^{18}O$ stack of ref. 43 to determine changes in deep-sea temperature (T_{ds}). A full copy of our PTC MathCad 13 worksheet, which was used to calculate the RSL_{Gib} relationship with eastern Mediterranean $\delta^{18}O$, as measured on the planktonic foraminiferal species *Globigerinoides ruber* (white) and *Neogloboquadrina pachyderma* (dextral), is available in Supplementary Information.

Online Content Any additional Methods, Extended Data display items and Source Data are available in the online version of the paper; references unique to these sections appear only in the online paper.

Received 13 November 2013; accepted 4 March 2014.
Published online 16 April 2014.

1. Rohling, E. J. *et al.* Antarctic temperature and global sea level closely coupled over the past five glacial cycles. *Nature Geosci.* **2,** 500–504 (2009).
2. Naish, T. *et al.* Obliquity-paced Pliocene West Antarctic ice sheet oscillations. *Nature* **458,** 322–328 (2009).
3. Miller, K. G. *et al.* High tide of the warm Pliocene: implications of global sea level for Antarctic deglaciation. *Geology* **40,** 407–410 (2012).
4. Foster, G. L. & Rohling, E. J. The relationship between sea level and climate forcing by CO_2 on geological timescales. *Proc. Natl Acad. Sci. USA* **110,** 1209–1214 (2013).
5. Sigman, D. M., Jaccard, S. & Haug, G. H. Polar ocean stratification in a cold climate. *Nature* **428,** 59–63 (2004).
6. Lawrence, K. T., Herbert, T. D., Brown, C. M., Raymo, M. E. & Haywood, A. M. High amplitude variations in North Atlantic sea surface temperature during the early Pliocene warm period. *Paleoceanography* **24,** PA2218 (2009).
7. Balco, G. & Rovey, C. W. II Absolute chronology for major Pleistocene advances of the Laurentide ice sheet. *Geology* **38,** 795–798 (2010).
8. Bailey, I. *et al.* An alternative suggestion for the Pliocene onset of major northern hemisphere glaciation based on the geochemical provenance of North Atlantic Ocean ice-rafted debris. *Quat. Sci. Rev.* **75,** 181–194 (2013).
9. Waelbroeck, C. *et al.* Sea-level and deep water temperature changes derived from benthic foraminifera isotopic records. *Quat. Sci. Rev.* **21,** 295–305 (2002).
10. Siddall, M. *et al.* Sea-level fluctuations during the last glacial cycle. *Nature* **423,** 853–858 (2003).
11. Grant, K. M. *et al.* Rapid coupling between ice volume and polar temperature over the past 150 kyr. *Nature* **491,** 744–747 (2012).
12. de Boer, B., Van de Wal, R. S. W., Bintanja, R., Lourens, L. J. & Tuenter, E. Cenozoic global ice-volume and temperature simulations with 1-D ice-sheet models forced by benthic $\delta^{18}O$ records. *Ann. Glaciol.* **51,** 23–33 (2010).
13. Miller, K. G. *et al.* The Phanerozoic record of global sea-level change. *Science* **310,** 1293–1298 (2005).
14. Elderfield, H. *et al.* Evolution of ocean temperature and ice volume through the Mid-Pleistocene Climate Transition. *Science* **337,** 704–709 (2012).
15. Sosdian, S. & Rosenthal, Y. Deep-sea temperature and ice volume changes across the Pliocene-Pleistocene climate transitions. *Science* **325,** 306–310 (2009).
16. Yu, J. & Broecker, W. S. Comment on "Deep-sea temperature and ice volume changes across the Pliocene-Pleistocene climate transitions". *Science* **328,** 1480c (2010).
17. Siddall, M. *et al.* Understanding the Red Sea response to sea level. *Earth Planet. Sci. Lett.* **225,** 421–434 (2004).
18. Rohling, E. J. Environmental controls on salinity and $\delta^{18}O$ in the Mediterranean. *Paleoceanography* **14,** 706–715 (1999).
19. Rohling, E. J. *et al.* Reconstructing past planktic foraminiferal habitats using stable isotope data: a case history for Mediterranean sapropel S5. *Mar. Micropaleontol.* **50,** 89–123 (2004).
20. Lourens, L. J. *et al.* Evaluation of the Plio-Pleistocene astronomical timescale. *Paleoceanography* **11,** 391–413 (1996).
21. Emeis, K.-C., Sakamoto, T., Wehausen, R. & Brumsack, H.-J. The sapropel record of the eastern Mediterranean Sea — results of Ocean Drilling Program Leg 160. *Palaeogeogr. Palaeoclimatol. Palaeoecol.* **158,** 371–395 (2000).
22. Wang, P., Tian, J. & Lourens, L. J. Obscuring of long eccentricity cyclicity in Pleistocene oceanic carbon isotope records. *Earth Planet. Sci. Lett.* **290,** 319–330 (2010).
23. Lourens, L. J., Wehausen, R. & Brumsack, H.-J. Geological constraints on tidal dissipation and dynamical ellipticity of the Earth over the past three million years. *Nature* **409,** 1029–1033 (2001).
24. Rohling, E. J. Quantitative assessment of glacial fluctuations in the level of Lake Lisan, Dead Sea rift. *Quat. Sci. Rev.* **70,** 63–72 (2013).
25. Rohling, E. J. Review and new aspects concerning the formation of Mediterranean sapropels. *Mar. Geol.* **122,** 1–28 (1994).
26. Jorissen, F. J. Benthic foraminiferal successions across Late Quaternary Mediterranean sapropels. *Mar. Geol.* **153,** 91–101 (1999).
27. Thomson, J., Mercone, D., De Lange, G. J. & Van Santvoort, P. J. M. Review of recent advances in the interpretation of eastern Mediterranean sapropel S1 from geochemical evidence. *Mar. Geol.* **153,** 77–89 (1999).
28. Mercone, D. *et al.* High-resolution geochemical and micropalaeontological probing of the most recent eastern Mediterranean sapropel. *Mar. Geol.* **177,** 25–44 (2001).
29. De Lange, G. J. *et al.* Synchronous basin-wide formation and redox-controlled preservation of a Mediterranean sapropel. *Nature Geosci.* **1,** 606–610 (2008).
30. Bryden, H. L. & Kinder, T. H. Steady two-layer exchange through the Strait of Gibraltar. *Deep Sea Res. I* **38,** S445–S463 (1991).
31. Rohling, E. J. & Bryden, H. L. Estimating past changes in the eastern Mediterranean freshwater budget, using reconstructions of sea level and hydrography. *Proc. Kon. Ned. Akad. B* **97,** 201–217 (1994).
32. Myers, P., Haines, K. & Rohling, E. J. Modelling the paleo-circulation of the Mediterranean: the last glacial maximum and the Holocene with emphasis on the formation of sapropel S1. *Paleoceanography* **13,** 586–606 (1998).
33. Matthiesen, S. & Haines, K. A hydraulic box model study of the Mediterranean response to postglacial sea-level rise. *Paleoceanography* **18,** 1084 (2003).
34. Mikolajewicz, U. Modelling Mediterranean ocean climate of the Last Glacial Maximum. *Clim. Past* **7,** 161–180 (2011).
35. Rogerson, M., Bigg, G. R., Rohling, E. J. & Ramirez, J. Vertical density gradient in the eastern North Atlantic during the last 30,000 years. *Clim. Dyn.* **39,** 589–598 (2012).
36. Loget, N. & Van der Driessche, J. On the origin of the Strait of Gibraltar. *Sedim. Geol.* **188–189,** 341–356 (2006).
37. Garcia-Castellanos, D. & Villaseñor, A. Messinian salinity crisis regulated by competing tectonics and erosion at the Gibraltar arc. *Nature* **480,** 359–363 (2011).
38. Hernández-Molina, F. J. *et al.* Contourite processes associated with the Mediterranean outflow water after its exit from the Strait of Gibraltar: global and conceptual implications. *Geology* **42,** 227–230 (2014).
39. Raymo, M. E., Mitrovica, J. X., O'Leary, M. J., DeConto, R. M. & Hearty, P. J. Departures from eustasy in Pliocene sea-level records. *Nature Geosci.* **4,** 328–332 (2011).
40. Rohling, E. J. *et al.* Comparison between Holocene and Marine Isotope Stage-11 sea-level histories. *Earth Planet. Sci. Lett.* **291,** 97–105 (2010).
41. Schrag, D. P., Hampt, G. & Murray, D. W. Pore fluid constraints on the temperature and oxygen isotopic composition of the glacial ocean. *Science* **272,** 1930–1932 (1996).
42. Adkins, J. F., McIntyre, K. & Schrag, D. P. The salinity, temperature, and $\delta^{18}O$ of the glacial deep ocean. *Science* **298,** 1769–1773 (2002).
43. Lisiecki, L. E. & Raymo, M. E. A Pliocene-Pleistocene stack of 57 globally distributed benthic $\delta^{18}O$ records. *Paleoceanography* **20,** PA1003 http://dx.doi.org/10.1029/2004PA001071 (2005).
44. Shackleton, N. J. & Opdyke, N. D. Oxygen isotope and palaeomagnetic evidence for early Northern Hemisphere glaciation. *Nature* **270,** 216–219 (1977).
45. Medina-Elizalde, M., Lea, D. W. & Fantle, M. S. Implications of seawater Mg/Ca variability for Plio-Pleistocene tropical climate reconstruction. *Earth Planet. Sci. Lett.* **269,** 585–595 (2008).
46. Seki, O. *et al.* Alkenone and boron-based Pliocene pCO_2 records. *Earth Planet. Sci. Lett.* **292,** 201–211 (2010).
47. Sigman, D. M., Hain, M. P. & Haug, G. H. The polar ocean and glacial cycles in atmospheric CO_2 concentration. *Nature* **466,** 47–55 (2010).
48. Herbert, T. D., Cleaveland Peterson, L., Lawrence, K. T. & Liu, Z. Tropical ocean temperatures over the past 3.5 million years. *Science* **328,** 1530–1534 (2010).
49. Clark, P. U. & Pollard, D. Origin of the middle Pleistocene transition by ice sheet erosion of regolith. *Paleoceanography* **13,** 1–9 (1998).
50. Bailey, I. *et al.* A low threshold for North Atlantic ice rafting from "low-slung slippery" late Pliocene ice sheets. *Paleoceanography* **25,** PA1212 (2010).

Supplementary Information is available in the online version of the paper.

Acknowledgements We thank M. Raymo for discussion of Pliocene sea-level estimates at the PALSEA2 workshop in Rome, October 2013, and all colleagues who made their data available—for example, via the PANGAEA and NOAA-NCDC Palaeoclimate data centres, or directly. This study was supported by 2012 Australian Laureate Fellowship FL120100050 (E.J.R.) and UK Natural Environment Research Council (NERC) consortium project iGlass (E.J.R., M.T., F.W., A.P.R.). F.W. acknowledges an Australian Bicentennial Scholarship Award from the Menzies Centre for Australian Studies, King's College London.

Author Contributions E.J.R. led the study, and performed the calculations. F.W. contributed the assessment of isostatic effects under the guidance of M.T. All authors contributed specialist insights to the discussions and helped with composing and refining the manuscript.

Author Information Reprints and permissions information is available at www.nature.com/reprints. The authors declare no competing financial interests. Readers are welcome to comment on the online version of the paper. Correspondence and requests for materials should be addressed to E.J.R. (eelco.rohling@anu.edu.au).

METHODS

Mediterranean RSL_{Gib} calculations. Philosophy. Our new Mediterranean RSL_{Gib} calculations follow the same philosophy as previous Red Sea RSL at Bab-el-Mandab (RSL_{BeM}) calculations[10,17]. RSL_{BeM} reconstructions rely on hydraulic control of water exchange through a shallow and narrow connection with the open ocean (the Bab-el-Mandab Strait)[10,17,51]. Sea-level lowering reduces this exchange and so increases the residence time of water in the highly evaporative sea, which causes strong increases in salinity and $\delta^{18}O$ of basin waters (the latter is reflected in carbonate microfossil $\delta^{18}O$). Quantification of the relationship between change in microfossil $\delta^{18}O$ and sea-level change then allows translation of such $\delta^{18}O$ records into sea-level time series[10,17,52]. The method yields RSL_{BeM} reconstructions with a 1σ uncertainty of ~6 m (RSL because it is uncorrected for local land movement). Propagation of these uncertainties along with chronological uncertainties gives a maximum-probability reconstruction of RSL_{BeM} with a 95% probability interval of ~3.5 m (ref. 11).

Identification of sapropelic intervals. Before eastern Mediterranean planktonic foraminiferal $\delta^{18}O$ records can be evaluated in terms of RSL_{Gib}, 'sapropel' intervals associated with major surface freshwater dilution (see main text) need to be removed. When sampling sediment core LC21 (Fig. 1a) for the study of Grant *et al.*[11], we kept records of the exact samples affected by such conditions (using colour, core-scanning X-ray fluorescence (XRF), and magnetic data, in addition to stable isotope, organic carbon, and microfossil abundance data from previous studies (for example, refs 19, 53–60), and manually excluded them on that basis. For the 5.3 Myr eastern Mediterranean $\delta^{18}O$ stack[22], we have no such exact documentation. Therefore, we removed sapropel intervals from that record using a signal processing approach. This involved (1) linearly detrending the stack; (2) identifying the long underlying eccentricity-frequency components in the detrended stack (using band-pass filtering); and (3) identifying sustained anomalies (sapropels) on shorter orbital frequencies, based on upcrossings through a level of 3× the standard deviation of short-term (sub-10-kyr period) 'noise' above the long-term component determined in (2) above. This approach is simplified but similar to one used to identify aeolian dust anomalies in Greenland ice-core records[61]. We then refined this processes by additional exclusion of samples based on reported ages of (visible) sapropel intervals on a related chronology[62], and we compare results with another sapropel-chronology[21] (Extended Data Fig. 1). The overall result is validated by agreement between iden>tified sapropel intervals and (high) Ba/Al anomalies in XRF scans of Ocean Drilling Program (ODP) Site 967 cores, which contribute to the Wang *et al.* Mediterranean stack (Extended Data Fig. 1). We identify three intervals where our signal-processing approach may not have filtered out $\delta^{18}O$ anomalies relating to sapropel events (yellow bars in Extended Data Fig. 1, and Figs 1 and 2).

Quantification of RSL_{Gib} from eastern Mediterranean planktonic foraminiferal $\delta^{18}O$ in non-sapropelic intervals. Here we describe the theoretical basis and steps of our procedure. For technical details, we refer to the copy of our PTC MathCad 13 worksheet in Supplementary Information.

Our calculations use a combination of the Bryden and Kinder[30] hydraulic control model for the Strait of Gibraltar with responses to variable sea-level and buoyancy forcing[31,63,64], with previously detailed Mediterranean evaporation and oxygen isotope fractionation equations[18,19]. Changes in the depth of the pycnocline at the top of the Mediterranean Intermediate Water (MIW) are parameterized as a function of changes in Gibraltar exchange and buoyancy forcing over the basin[25,31]. The Mediterranean box model used here is an amended version of that developed previously for Mediterranean planktonic foraminiferal habitat characterizations and monsoon runoff estimation[19], which now includes the effects of sea-level change (compare refs 18, 31). Summer mixed layer depth is set (after Nykjaer[65]) to 30 + *rnd*(5) m, where the term *rnd*(5) stands for a random value from a normal distribution with a 3σ range of ±5 m. In contrast to Rohling *et al.*[19], we do not consider a separate monsoon-freshwater-influx box within the summer period, because that was specific to the assessment of influences of freshwater lenses during times of sapropel formation, which are excluded here. The boxes of particular interest here are the summer mixed-layer box (for *Globigerinoides ruber* (white)) and the intermediate water box (for *Neogloboquadrina pachyderma* (dextral))[19].

Evaporation is calculated using bulk evaporation formulae, and we use parameterizations for runoff and precipitation proportions during non-sapropel periods that are based on present-day observations with an added random (and uncorrelated) uncertainty range (3σ) of ~10%. Basin temperatures are set to covary with sea-level change (glaciation state) with glacial–interglacial gradients of 5 + *rnd*(1) and 3.5 + *rnd*(1) °C per 120 m sea-level change for summer and winter, respectively, based on reconstructions of Last Glacial Maximum-to-Present gradients[66]. The gradients are applied relative to modern values of 22 and 16 °C (refs 65, 67). Net freshwater runoff from the Black Sea is taken as 1 + *rnd*(0.1) times the present-day (pre-damming) value after Tolmazin[68], and is reduced to zero when sea level stands below –80 m (the approximate depth of the connecting straits). Regardless, this term has negligible impact on the solutions presented. Relative humidity over the basin is taken at 0.70 + *rnd*(0.05) (ref. 18), which reflects the fact that the Mediterranean basin has always been at the same geographic position, landlocked, and influenced by continental airflows, throughout the period of time considered. Oxygen isotope fractionation is calculated exactly as detailed in Rohling *et al.*[19]. We calculate O-isotope ratios in water relative to Standard Mean Ocean Water (SMOW), and carbonate (microfossil) isotope ratios are expressed relative to the Vienna Pee Dee Belemnite standard (VPDB) (conversions are included in our code; see Supplementary Information). The $\delta^{18}O$ of inflowing Atlantic water is changed as a function of sea level, using a ratio of 0.009‰ m^{-1} (refs 14, 41, 42). We have assumed that there has been no net heat gain or loss in the Mediterranean, as is approximately the case today given that inflow and outflow are nearly at the same temperature[30]. This is a necessary assumption, which can only be refined if long and highly resolved temperature records of high (~0.1 °C) precision are developed for both the Atlantic and Mediterranean waters that exchange through the Strait of Gibraltar.

Many of the input parameters cannot be accurately estimated for the past. Therefore, we have allowed substantial random variations in all terms, so that we obtain a solution for the $\delta^{18}O$-to-RSL 'converters' (the RSL sensitivity of $\delta^{18}O$ for eastern Mediterranean sites) that fully propagates the parameter uncertainties into a realistic end-product uncertainty. Future research may help to reduce some of these uncertainties. Any major change to the two fundamental underlying assumptions (for discussion, see main text, and below) is expected to systematically invalidate the converters for certain times in the past, and mutual validation with independent sea-level methods would highlight if this is the case. It appears, however, that our solution consistently gives sea-level amplitude variations that are comparable with those from independent observation-based methods, back to ~3.4 Myr ago (Fig. 2). Hence, we infer that the underlying assumptions are sufficiently valid back to ~3.4 Myr ago, but further research is needed to strengthen/detail this, especially in the pre-3.4-Myr interval.

Our end-products are two planktonic foraminiferal $\delta^{18}O$-to-RSL converters, for *G. ruber* (white) and *N. pachyderma* (dextral), respectively. We have approximated each converter (including its uncertainty intervals) with polynomial fits (Extended Data Fig. 2); the latter can easily be applied to relevant microfossil $\delta^{18}O$ records, after normalization of these $\delta^{18}O$ records to an interval of known sea level (for example, the present). We have normalized records to their mean value for the interval 0–3 kyr ago, and impose that this level corresponds to RSL_{Gib} = ~0 m.

We next perform a probabilistic assessment of the reconstructed RSL_{Gib} record. This takes into account the methodological uncertainty as determined above, along with a chronological uncertainty. The latter is set to a uniform 3σ range of ±4–5 kyr (owing to orbital tuning as well as creation of the stack). After 500 samplings of the data within the described (assumed normal) distributions for sea level and age, we then performed simple linear interpolation between the points in each case (also across the sapropel gaps). Per time step of 1 kyr, we then determined the probability density distribution for sea level, identifying the median along with its 95% probability interval (approximately equivalent to 2 s.e.), as well as the 68% (16th–84th percentile), 95% (2.5th–97.5th percentile), and 99% (0.5th–99.5th percentile) intervals for the data. For more detail on this approach, see ref. 11. Although our method includes all known sources of uncertainty, we cannot yet include tectonic uncertainties.

Tectonic considerations. Large-scale geophysical processes are thought to have played an important role in the isolating the Mediterranean from the open ocean during the Messinian Salinity Crisis (MSC), and in its eventual reconnection through development of the passage that now is the Strait of Gibraltar (see, for example, refs 37, 69). Ref. 69 argues that such processes are essential because there would be no case for an ESL drop at the onset of the MSC, but this notion has been challenged by recent reports of a distinct sea-level drop coincident with the MSC onset[70]. Viewed in a wider context than just the MSC, it seems that subsidence might be expected in the strait region (1) especially in the early Pliocene owing to rollback and steepening of the subsiding Gibraltar slab; and (2) throughout the Plio-Pleistocene owing to sediment loading in marine basins around the Strait since reconnection to the Atlantic Ocean (for processes, see ref. 69, and—for a nearby region—ref. 71). However, long-term uplift can also be expected in the region, owing to the overall convergence between Iberia and Africa[69]. It is challenging to quantify the temporal history of either magnitude, or sign, of these long-term vertical movements from existing data. However, it seems at least clear from sedimentological data that water exchange through the Strait of Gibraltar settled into a modern-type pattern from about 3.8 Myr ago, with outflow creating a sequence of contourite deposits in the Gulf of Cadiz that remains active today[38]. This strengthens confidence in our assumption of approximately analogous tectono-geophysical conditions over the past ~3.8 Myr.

Further insight into long-term vertical movements at the strait may be obtained from mutual validations of RSL_{Gib} against independent data, with respect to both absolute sea level and sea-level amplitude variability (that is, if the Strait of Gibraltar were fundamentally different than today, the sea-level sensitivity would be different). As discussed previously, and in the main text, validations are promising down to ~3.4 Myr, which suggests limited impact from tectonic changes at least back to that time. As independent sea-level records become available that extend to older times (3–5.3 Myr ago), any discrepancies relative to RSL_{Gib} may help to further understand the uplift history of the region.

Isostatic effects. Our method delivers RSL estimates at the Strait of Gibraltar. Isostatic corrections are needed to allow comparison in detail with eustatic sea-level (ESL) information (for example, deconvolutions of deep-sea $\delta^{18}O_b$ that approximate ice volume). However, little is known about long-timescale isostatic corrections; first explorations were presented only recently[39]. For a preliminary assessment of isostatic adjustment at the Camarinal sill, we created a simulated ice-loading history over two full glacial cycles by duplicating the ICE-5G ice-model history[72] around a 4,000-year interglacial period with near present-day ice volume, with no adjustment made to the geographical distribution of ice within ICE-5G. The Earth response was parameterized over three lithospheric thicknesses (71, 96 and 120 km) and a range of upper and lower mantle viscosities (1×10^{20} to 1×10^{21} Pa s, and 2×10^{21} to 5×10^{22} Pa s, respectively). A range of 495 combinations was examined, using a glacial isostatic adjustment model that incorporates principles described by Kendall *et al.*[73].

Results are shown in Extended Data Figs 3 and 4. Our analysis suggests that the glacial–interglacial amplitude of RSL_{Gib} probably underestimates global mean ESL change by 20–25% at glacial maxima. The offset between RSL_{Gib} and ESL is not constant over time, but scales proportionally with land-ice variations, giving a linear relationship between global mean sea level and relative sea level: $ESL = (1.23 \pm 0.08)RSL_{Gib} + (0.5 \pm 1.9)$. The errors are expressed as two standard deviations. For RSL_{BeM}, the same model runs give rise to stronger hysteresis between responses for glaciation or deglaciation, but $ESL{:}RSL_{BeM}$ ratios overall are comparable to those for Gibraltar, ranging between 1.13 (glaciation) and 1.24 (deglaciation).

Future methodological refinements. There is considerable potential for (extensive) future work to refine the RSL_{Gib} method, both in terms of RSL uncertainty, and in terms of continuity through sapropelic intervals. Specifically, there are two key targets. First, the climatological analogue assumption of our method (see main text) may be validated and/or adjusted, using detailed quantitative reconstructions of Mediterranean climate conditions for different (especially Pliocene and early Pleistocene) periods of time within the past 5.3 Myr. Second, continuity through and close to sapropelic intervals may be improved through development of multiple replicated, centennial-scale resolution, eastern Mediterranean surface-water $\delta^{18}O_p$ records, with strictly co-registered (same-sample) sapropel-indicator data. Depending on progress, the 'monsoon box' in the model[19] may eventually be reinstated, to resolve RSL_{Gib} through sapropel intervals by quantifying hydrological impacts on Mediterranean $\delta^{18}O$ during these times. Note that this will likely require intensive data–model comparisons for each sapropelic interval considered[18,19].

Probabilistic assessment of the Elderfield *et al.*[14] sea-level record. We performed a probabilistic assessment of the sea-level record of Elderfield *et al.*[14] to ascertain its confidence levels, given that several sources of uncertainty would have been propagated into their sea-level record at each stage of its development. Based on the Mg/Ca range in the Mg/Ca to T_{ds} calibration of ref. 74 and the mean calibration slope (their figure 1), the 2σ T_{ds} range is ± 3 °C. In glacial intervals, the calibration is based on extrapolation into a region where no core-top data exist. This introduces extra uncertainty to T_{ds} reconstructions in cold intervals, but we ignore that component here because it is difficult to quantify. Calibration uncertainties are true random uncertainties; there also are further potential sources of truly random uncertainty that relate to the materials analysed and their statistical composition (each sample represents a random mixture of several centuries, presenting an average with considerable potential variability). In light of these unknowns, we assume that the only uncertainty in Mg/Ca-based T_{ds} is the random calibration uncertainty ($1\sigma = 1.5$ °C), which probably is the dominant term.

Based on 0.25‰ °C^{-1} for $\delta^{18}O$ changes in benthic foraminiferal carbonate ($\delta^{18}O_b$), a 1.5 °C T_{ds} uncertainty translates into ~0.35‰ uncertainty. The remaining (residual) component of change in the $\delta^{18}O_b$ signal was converted into estimates of sea-level change using a ratio of 0.01‰ m^{-1} (ref. 14); uncertainties for this ratio are typically 0.001‰ m^{-1} (1σ), or 10% of the inferred sea level (see main text). Therefore, the Elderfield *et al.*[14] sea-level reconstruction from Mg/Ca-based T_{ds} correction of $\delta^{18}O_b$ has uncertainties of ± 35 m (from the T_{ds} uncertainty) and ± 0.1SL (where SL indicates the sea level; from the sea-level-conversion uncertainty; both at 1σ). This gives the method a total uncertainty of about $35 + 0.1$SL m (1σ). This may appear large, but there is strong autocorrelation in the record, which leads to considerably tighter uncertainty limits to underlying 'mean' sea-level trends (see below).

We also consider chronological uncertainties in the ODP Site 1123 timescale used by Elderfield *et al.*[14]. Although their chronology does not fully rely on Lisiecki and Raymo[43], there is close agreement between these chronologies, which suggests similar (small) uncertainties. We therefore assign initial (random) chronological uncertainties according to Lisiecki and Raymo[43], who wrote:

"Including all sources of error, we estimate the uncertainty in the LR04 age model to be 40 ky from 5.3–5 Ma, 30 ky from 5–4 Ma, 15 ky from 4–3 Ma, 6 ky from 3–1 Ma, and 4 ky from 1–0 Ma."

We use these as symmetrical 1σ values (that is, 4 kyr equals ± 2 kyr). The exact initial values used are not so important, because the record of Elderfield *et al.*[14] was sampled in high resolution, and in a strictly contiguous, stratigraphic context, which strongly reduces chronological uncertainties in a relative sample-to-sample sense. Our assessment, therefore, includes propagation of age uncertainties but constrains this (within the initial uncertainty estimates) to a strictly imposed monotonic, stratigraphic sequence (that is, no age reversals are allowed).

We randomly sampled all individual data points 1,000 times within their sea-level and age uncertainties, based on normal distributions with a mean at the respective datapoint values and standard deviations as discussed above. We then linearly interpolated the records for each of the 1,000 iterations, and determined at set age intervals the probability density distribution for sea level. We determined the probability maximum (modal value) with its 95% probability interval (~equivalent to 2 s.e.), as well as the 68% (16th–84th percentile), 95% (2.5th–97.5th percentile), and 99% (0.5th–99.5th percentile) intervals for the data (approximating 1σ, 2σ and 3σ, but not necessarily symmetrically). For detail on this approach, see ref. 11. The resultant probability curve is shown in Fig. 2a.

Using RSL_{Gib} with the deep-sea $\delta^{18}O_b$ stack[43] to determine T_{ds}. For this exercise, we first approximate glacial–interglacial changes in mean ocean $\delta^{18}O$ ($\delta^{18}O_w$) using RSL_{Gib} and a conversion scaling of (0.009 ± 0.001)‰ m^{-1} (1σ) (refs 41, 42). Subtraction of these values from $\delta^{18}O_b$ changes gives a residual, which is due to T_{ds} changes following a ratio of 0.25‰ °C^{-1}. Prior to this subtraction, we fine-tuned the chronology of the deep-sea $\delta^{18}O_b$ stack[43] to that of the Mediterranean $\delta^{18}O_p$ stack[22], using graphic correlation guided by the orbitally tuned chronologies of the two stacks. Adjustments remained within the reported uncertainties[43]. Correlation tie-points used are listed in Extended Data Table 1.

51. Rohling, E. J. *et al.* Magnitudes of sea-level lowstands of the past 500,000 years. *Nature* **394,** 162–165 (1998).
52. Biton, E., Gildor, H. & Peltier, W. R. Relative sea level reduction at the Red Sea during the Last Glacial Maximum. *Paleoceanography* **23,** PA1214 (2008).
53. Mercone, D., Thomson, J., Abu-Zied, R. H., Croudace, I. W. & Rohling, E. J. High-resolution geochemical and micropalaeontological profiling of the most recent eastern Mediterranean sapropel. *Mar. Geol.* **177,** 25–44 (2001).
54. Marino, G. *et al.* Aegean Sea as driver for hydrological and ecological changes in the eastern Mediterranean. *Geology* **35,** 675–678 (2007).
55. Marino, G. *et al.* Early and middle Holocene in the Aegean Sea: interplay between high and low latitude climate variability. *Quat. Sci. Rev.* **28,** 3246–3262 (2009).
56. Rohling, E. J., Mayewski, P. A., Hayes, A., Abu-Zied, R. H. & Casford, J. S. L. Holocene atmosphere-ocean interactions: records from Greenland and the Aegean Sea. *Clim. Dyn.* **18,** 587–593 (2002).
57. Casford, J. S. L. *et al.* A dynamic concept for eastern Mediterranean circulation and oxygenation during sapropel formation. *Palaeogeogr. Palaeoclimatol. Palaeoecol.* **190,** 103–119 (2003).
58. Casford, J. S. L. *et al.* Circulation changes and nutrient concentrations in the Late Quaternary Aegean Sea: a non-steady state concept for sapropel formation. *Paleoceanography* **17,** http://dx.doi.org/10.1029/2000PA000601 (2002).
59. Casford, J. S. L. *et al.* A stratigraphically controlled multi-proxy chronostratigraphy for the eastern Mediterranean. *Paleoceanography* **22,** PA4215 (2007).
60. Osborne, A., Marino, G., Vance, D. & Rohling, E. J. Eastern Mediterranean surface water Nd during Eemian sapropel S5: monitoring northerly (mid latitude) versus southerly (sub tropical) freshwater contributions. *Quat. Sci. Rev.* **29,** 2473–2483 (2010).
61. Rohling, E. J., Mayewski, P. A. & Challenor, P. On the timing and mechanism of millennial-scale climate variability during the last glacial cycle. *Clim. Dyn.* **20,** 257–267 (2003).
62. Kroon, D. *et al.* Oxygen isotope and sapropel stratigraphy in the eastern Mediterranean during the last 3.2 million years. *Proc. ODP Sci. Res.* **160,** 181–189 (1998).
63. Rohling, E. J. A simple two-layered model for shoaling of the eastern Mediterranean pycnocline due to glacio-eustatic sea-level lowering. *Paleoceanography* **6,** 537–541 (1991).
64. Rohling, E. J. Shoaling of the eastern Mediterranean pycnocline due to reduction of excess evaporation: implications for sapropel formation. *Paleoceanography* **6,** 747–753 (1991b).
65. Nykjaer, L. Mediterranean Sea surface warming 1985–2006. *Clim. Res.* **39,** 11–17 (2009).
66. Hayes, A., Kucera, M., Kallel, N., Sbaffi, L. & Rohling, E. J. Glacial Mediterranean sea surface temperatures reconstructed from planktonic foraminiferal assemblages. *Quat. Sci. Rev.* **24,** 999–1016 (2005).
67. Stanev, E. V., Friedrich, H. J. & Botev, S. V. On the seasonal response of intermediate and deep water to surface forcing in the Mediterranean Sea. *Oceanol. Acta* **12,** 141–149 (1989).
68. Tolmazin, D. Changing coastal oceanography of the Black Sea. I: Northwestern shelf. *Prog. Oceanogr.* **15,** 217–276 (1985).

69. Govers, R. Choking the Mediterranean to dehydration: the Messinian Salinity Crisis. *Geology* **37,** 167–170 (2009).
70. Jiménez-Moreno, G. *et al.* Vegetation, sea-level, and climate changes during the Messinian salinity crisis. *Geol. Soc. Am. Bull.* **125,** 432–444 (2013).
71. Rabineau, M. *et al.* Quantifying subsidence and isostatic readjustment using sedimentary paleomarkers, example from the Gulf of Lion. *Earth Planet. Sci. Lett.* **388,** 353–366 (2014).
72. Peltier, W. R. Global glacial isostasy and the surface of the ice-age Earth: the ICE-5G (VM2) model and GRACE. *Annu. Rev. Earth Planet. Sci.* **32,** 111–149 (2004).
73. Kendall, R. A., Mitrovica, J. X. & Milne, G. A. On post-glacial sea level – II. Numerical formulation and comparative results on spherically symmetric models. *Geophys. J. Int.* **161,** 679–706 (2005).
74. Elderfield, H. *et al.* A record of bottom water temperature and seawater $\delta^{18}O$ for the Southern Ocean over the past 440 kyr based on Mg/Ca of benthic foraminiferal *Uvigerina* spp. *Quat. Sci. Rev.* **29,** 160–169 (2010).
75. McKay, R. *et al.* Antarctic and Southern ocean influences on late Pliocene global cooling. *Proc. Natl Acad. Sci. USA* **109,** 6423–6428 (2012).
76. Ravelo, A. C., Andreasen, D. H., Lyle, M., Lyle, A. O. & Wara, M. W. Regional climate shifts caused by gradual global cooling in the Pliocene epoch. *Nature* **429,** 263–267 (2004).
77. Hillenbrand, C.-D. & Cortese, G. Polar stratification: a critical view from the Southern Ocean. *Palaeogeogr. Palaeoclimatol. Palaeoecol.* **242,** 240–252 (2006).
78. Hodell, D. A. & Venz-Curtis, K. A. Late Neogene history of deepwater ventilation in the Southern Ocean. *Geochem. Geophys. Geosyst.* **7,** Q09001 (2006).
79. Naafs, B. D. A., Hefter, J. & Stein, R. Millennial-scale ice rafting events and Hudson Strait Heinrich(-like) events during the late Pliocene and Pleistocene: a review. *Quat. Sci. Rev.* **80,** 1–28 (2013).
80. Kleiven, H. F., Jansen, E., Fronval, T. & Smith, T. M. Intensification of Northern Hemisphere glaciations in the circum Atlantic region (3.5-2.4 Ma) — ice-rafted detritus evidence. *Palaeogeogr. Palaeoclimatol. Palaeoecol.* **184,** 213–223 (2002).
81. Knies, J. *et al.* The Plio-Pleistocene glaciation of the Barents Sea-Svalbard region: a new model based on revised chronostratigraphy. *Quat. Sci. Rev.* **28,** 812–829 (2009).
82. Mattingsdal, R. *et al.* A new 6 Myr stratigraphic framework for the Atlantic–Arctic Gateway. *Quat. Sci. Rev.* http://dx.doi.org/10.1016/j.quascirev.2013.08.022 (published online 19 September 2013).
83. Gebhardt, A. C., Geissler, W. H., Matthiessen, J. & Jokat, W. Changes in current patterns in the Fram Strait at the Pliocene/Pleistocene boundary. *Quat. Sci. Rev.* http://dx.doi.org/10.1016/j.quascirev.2013.07.015 (published online 3 August 2013).
84. Naafs, B. D. A. *et al.* Strengthening of North American dust sources during the late Pliocene (2.7 Ma). *Earth Planet. Sci. Lett.* **317–318,** 8–19 (2012).
85. Bailey, I. *et al.* Flux and provenance of ice-rafted debris in the earliest Pleistocene sub-polar North Atlantic Ocean comparable to the last glacial maximum. *Earth Planet. Sci. Lett.* **341–344,** 222–233 (2012).
86. Haug, G. H. *et al.* North Pacific seasonality and the glaciation of North America 2.7 million years ago. *Nature* **433,** 821–825 (2005).
87. Martínez-Garcia, A., Rosell-Mele, A., McClymont, E. L., Gersonde, R. & Haug, G. H. Subpolar link to the emergence of the modern equatorial Pacific cold tongue. *Science* **328,** 1550–1553 (2010).
88. Jansen, E. & Sjøholm, J. Reconstruction of glaciation over the past 6 Myr from ice-borne deposits in the Norwegian Sea. *Nature* **349,** 600–603 (1991).
89. Hodell, D. A. & Ciesielski, P. F. Stable isotopic and carbonate stratigraphy of the late Pliocene and Pleistocene of Hole 704A: eastern subantarctic South Atlantic. *Proc. ODP Sci. Res.* **114,** 409–435 (1991).
90. Shackleton, N. J. *et al.* Oxygen isotope calibration of the onset of ice-rafting and history of glaciation in the North Atlantic region. *Nature* **307,** 620–623 (1984).
91. Allen, C. P. & Warnke, D. A. History of ice rafting at Leg 114 sites, subantarctic/South Atlantic. *Proc. ODP Sci. Res.* **114,** 599–607 (1991).
92. Haley, B. A., Frank, M., Spielhagen, R. F. & Eisenhauer, A. Influence of brine formation on Arctic Ocean circulation over the past 15 million years. *Nature Geosci.* **1,** 68–72 (2008).
93. Butt, F. A., Elverhoi, A., Solheim, A. & Forsberg, C. F. Deciphering late Cenozoic development of the western Svalbard margin from ODP site 986 results. *Mar. Geol.* **169,** 373–390 (2000).
94. Shackleton, N. J. & Opdyke, N. D. Oxygen isotope and palaeomagnetic evidence for early Northern Hemisphere glaciation. *Nature* **270,** 216–219 (1977).
95. Raymo, M. E., Ruddiman, W. F., Backman, J., Clement, B. M. & Martinson, D. G. Late Pliocene variation in Northern Hemisphere ice sheets and North Atlantic deep water circulation. *Paleoceanography* **4,** 413–446 (1989).
96. Tiedemann, R., Sarnthein, M. & Shackleton, N. J. Astronomic timescale for the Pliocene Atlantic $\delta^{18}O$ and dust flux records of Ocean Drilling Program Site 659. *Paleoceanography* **9,** 619–638 (1994).
97. Haug, G. H. & Tiedemann, R. Effect of the formation of the Isthmus of Panama on Atlantic Ocean thermohaline circulation. *Nature* **393,** 673–676 (1998).
98. Lisiecki, L. E. & Raymo, M. E. Plio-Pleistocene climate evolution: trends and transitions in glacial cycle dynamics. *Quat. Sci. Rev.* **26,** 56–69 (2007).
99. Mudelsee, M. & Raymo, M. E. Slow dynamics of the Northern Hemisphere glaciation. *Paleoceanography* **20,** PA4022 (2005).

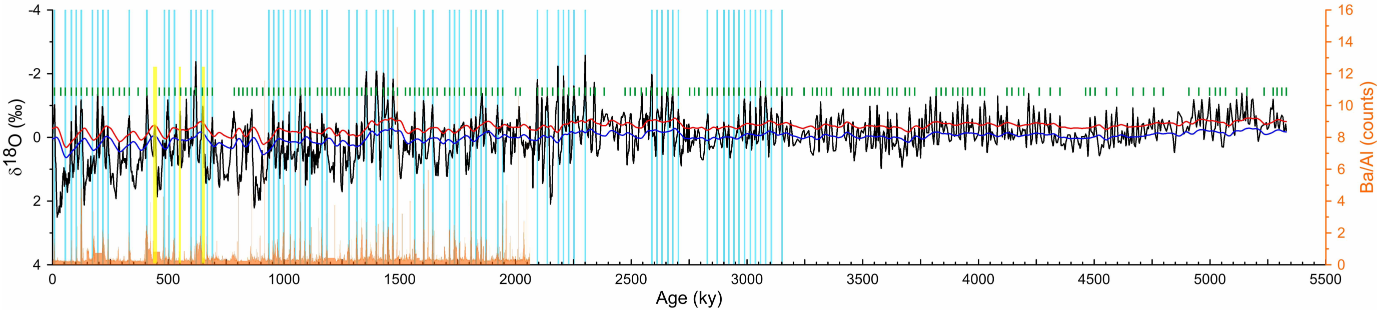

Extended Data Figure 1 | Summary of our sapropel detection method. A mean-normalized version of the eastern Mediterranean $\delta^{18}O$ stack[22] after linear detrending (black; left-hand *y* axis) is shown along with preliminary core-scanner XRF Ba/Al data for ODP Site 967 (orange; right-hand *y* axis). Also shown are eastern Mediterranean sapropel intervals according to the chronology of Kroon *et al.*[62] (vertical blue bars), and according to Emeis *et al.*[21] (vertical green dashes). Note that minor chronological differences may exist relative to Wang *et al.*[22], and that previous sapropel recognition[21,62] was mainly done on the basis of colour. Also shown are the eccentricity-related component in the Mediterranean $\delta^{18}O$ stack based on two rectangular bandpass filters for periods of 80–130 kyr and 360–440 kyr (dark blue), and our upcrossing cut-off criterion based on the eccentricity-related component plus 3 standard deviations of short-term (sub-10-kyr) variability (red). The yellow bars indicate three sapropel(-like) intervals that were not detected with this method, but which are apparent compared to other methods (main text).

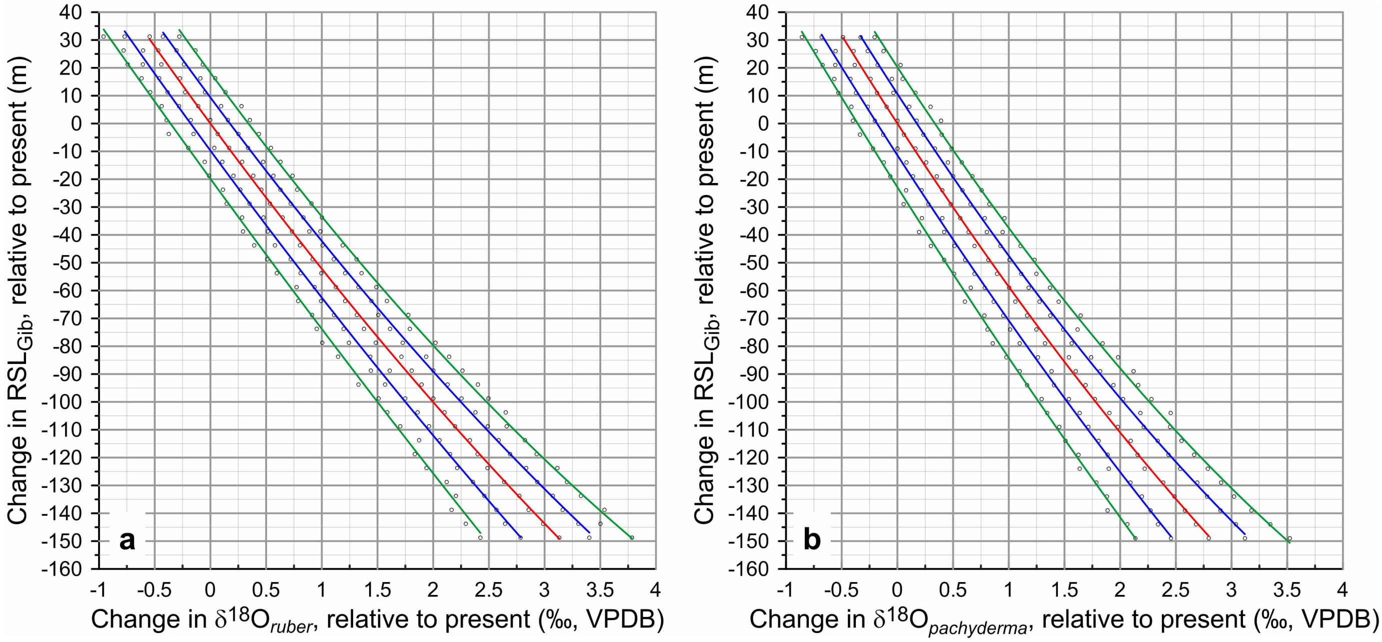

Extended Data Figure 2 | δ^{18}O-to-RSL 'converters' calculated in the present study. **a**, For *G. ruber* (white). **b**, For *N. pachyderma* (dextral). Data are shown with polynomial fits for: the mean (red), 68% probability limits (blue) and 95% probability limits (green). Equations (below) for the polynomial fits are those used to establish RSL_{Gib} changes from eastern Mediterranean δ^{18}O changes. For *G. ruber* (white), the fit equations are (from top/right to bottom/left): $y = 18.23253367 - 54.32756406x + 2.68013962x^2$, $y = 9.359718967 - 53.88724018x + 2.336521849x^2$, $y = -54.33006067x + 2.144129497x^2$, $y = -9.721121814 - 54.4447188x + 1.639979972x^2$, and $y = -19.83859107 - 54.97329064x + 1.027303677x^2$. For *N. pachyderma* (dextral), the fit equations are (from top/right to bottom/left): $y = 20.27152514 - 61.45134479x + 3.673345939x^2$, $y = 10.65608987 - 61.68573435x + 3.521130244x^2$, $y = -61.74158411x + 3.12127659x^2$, $y = -11.37304383 - 61.90236624x + 2.499068186x^2$, and $y = -22.84772173 - 63.3490518x + 2.014759373x^2$.

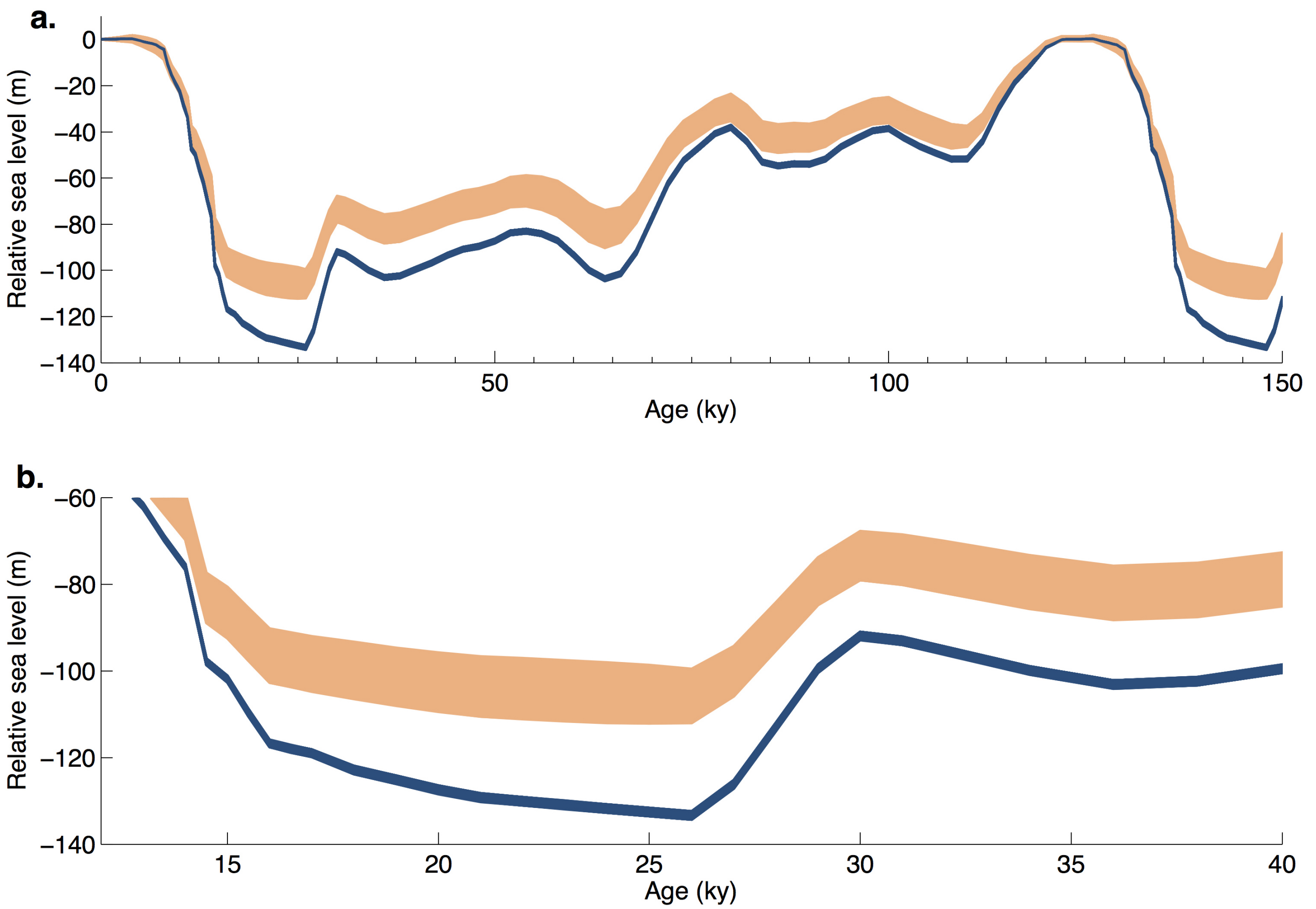

Extended Data Figure 3 | Preliminary isostatic assessment results for the Camarinal sill, the critical location of water-exchange control for the Strait of Gibraltar. **a**, Over the past 150 kyr. **b**, Magnified for the past 40 kyr. Orange is the range of modelled RSL, blue is the range of associated global mean (eustatic) sea levels (ESL). The graph illustrates that RSL_{Gib} is—to a first approximation over the long timescales considered in the present study—related to ESL through a ratio that is relatively constant over the range of sea levels considered (see also Extended Data Fig. 4 and Methods).

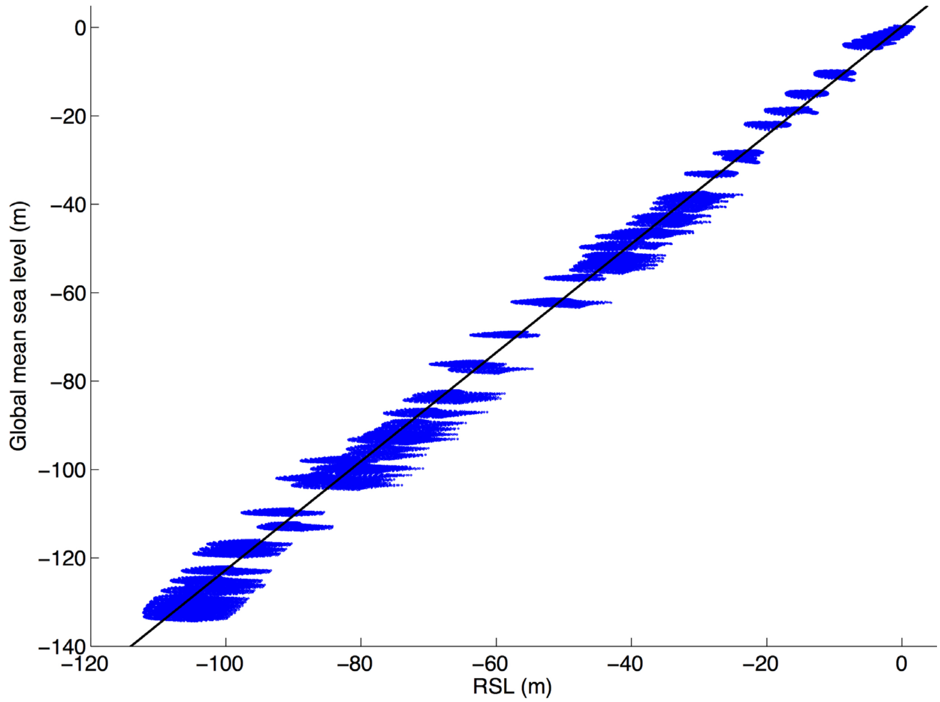

Extended Data Figure 4 | Global mean ESL versus RSL_{Gib} over the full range of 495 Earth model configurations considered. This reveals that, to a first approximation, ESL = 1.23 RSL_{Gib}, with a 95% probability interval on the slope value between 1.15 and 1.31.

Extended Data Table 1 | Tie-points between the Lisiecki and Raymo[43] and Wang *et al.*[22] chronologies

Age (ky) Ref.43	Age (ky) Ref.22
0.00	0.00
12.63	15.18
131.68	132.38
244.85	246.85
335.85	338.53
421.43	427.88
619.89	625.73
677.37	683.37
743.02	736.06
789.82	795.59
866.23	866.12
1189.58	1189.11
1492.49	1494.79
1865.33	1864.12
1941.17	1942.56
2020.79	1999.96
2070.55	2075.56
2197.62	2188.93
2330.78	2333.65
2369.64	2365.44
2492.14	2491.57
2511.60	2505.23
2535.25	2531.80
2795.07	2796.31
2938.41	2952.57
3054.56	3051.87
3123.94	3091.74
3262.63	3268.78
3303.45	3292.07
3658.89	3656.27
3863.33	3868.85
3990.95	3980.89
4397.68	4400.03
4486.16	4513.22
4841.62	4840.82
5037.74	5047.62
5171.02	5203.70

Extended Data Table 2 | Other evidence of late Pliocene climate change

Time (My)	Observation	Proxy	Ref.
3.3-2.6	Southern Ocean cooling; development of Antarctic sea ice	Lithofacies, $\delta^{15}N$, $\delta^{13}C$	75
3.0-2.5	Deep ocean cooling in the North Atlantic	Mg/Ca	15
~3.0	Thermocline shoaling in the subtropical North Pacific	$CaCO_3$ MARs, planktic $\delta^{13}C$	76
3.3-2.3	Decrease/increase in biogenic silica accumulation in the Antarctic Zone/Subantarctic Front	Biogenic opal	77
2.8-2.6	Surface water cooling in the North Atlantic	UK'37	6
~2.8	Decrease in Southern Ocean ventilation	Benthic $\delta^{13}C$	78
2.75	First ice-rafting in North Atlantic mid-latitudes	IRD	79
~2.7	Glacial intensification in the circum-Atlantic region	IRD, clays	80,81
~2.7	Svalbard ice sheet reached shelf break; increased glacial erosion	Seismic profiles	82
~2.7	Ice sheet expansion in the northern Barents Sea	Seismic profiles	83
~2.7	Increased aeolian inputs to the North Atlantic	n-alkanes, n-alkanl-1-ols	84
~2.75	Increased dust, ash and IRD to the North Pacific	IRD, magnetics	85
2.7	Development of the North Pacific halocline	$\delta^{15}N$, opal MARs	5
2.7	Increased stratification in the Subarctic Pacific	UK'37, planktic $\delta^{18}O$	86
~2.7	First significant increase in dust inputs to the Southern Ocean	Fe MARS, n-alkanes	87
2.64	Onset of major NHG (including northeast America)	IRD geochemistry	8
2.57	Onset of extensive glaciation in northern Europe	IRD	88
~2.55	Significant ice-sheet calving into the North Pacific	IRD	85
2.47	Change in Polar Front dynamics in the Subantarctic South Atlantic	Planktic and benthic $\delta^{18}O$, $\delta^{13}C$; $CaCO_3$ %	89
2.4	First major ice rafting in the North Atlantic	IRD	90*
2.5-2.2	Significant ice rafting to the Subantarctic South Atlantic	IRD	91
~2.0	Arctic Intermediate Water changes (linked to growth of first major North Eurasian ice sheets)	εNd	92
2.4-1.0	Southward expansion of Barents Sea ice sheet	IRD, clays	81
2.3-1.6	Initial glacial growth on Svalbard margin	Grain size, geochemistry	93
Deep-sea $\delta^{18}O_b$-based inferences			
2.5	Major change in the character of glaciations	Benthic $\delta^{18}O$	94*
2.95-2.4	Gradual increase in ice volume	Benthic $\delta^{18}O$	95
3.15-2.5	Major ice-volume increase	Benthic $\delta^{18}O$	96
3.1-2.5	Pronounced intensification of NHG	Benthic $\delta^{18}O$	97
2.7	Onset of NHG	Benthic $\delta^{18}O$ stack	43,98
3.6-2.4	Long-term development of NHG	planktonic and benthic $\delta^{18}O$	99

Data sources[75–99] shown in rightmost column. MAR, mass accumulation rate; IRD, ice-rafted debris; NHG, Northern Hemisphere glaciation.
* Chronology of early papers (pre-astronomical tuning) may be too young by a few hundred kyr, so that 2.4/2.5 Myr ago in the older studies is closer to 2.6/2.7 Myr ago in astronomically tuned chronologies.

CORRECTIONS & AMENDMENTS

CORRIGENDUM

doi:10.1038/nature13488

Corrigendum: Sea-level and deep-sea-temperature variability over the past 5.3 million years

E. J. Rohling, G. L. Foster, K. M. Grant, G. Marino, A. P. Roberts, M. E. Tamisiea & F. Williams

Nature **508,** 477–482 (2014); doi:10.1038/nature13230

In this Article, owing to a misunderstanding of discussions at the PALSEA2 workshop in Rome, we erroneously reported previous sea-level estimates for the period 3.3–2.9 Myr as originating from the 'Pliocene Maximum Sea Level' (PLIOMAX) project. However, these estimates are not from PLIOMAX, relating to ref. 3 instead. We thank M. E. Raymo and A. Rovere for drawing the error to our attention. The online versions of the paper have been corrected.